Visualization of Millimeter-Wave Radio Signals Utilizing Measured Radio Channel Parameters

Petersen, Sigurd Sándor; Feldstedt, Oskar Kjul; Guled, Khadar; Fan, Wei

Published in:
2022 IEEE Conference on Antenna Measurements and Applications (CAMA)

DOI (link to publication from Publisher):
10.1109/CAMA56352.2022.10002610

Publication date:
2022

Document Version
Accepted author manuscript, peer reviewed version

Visualization of Millimeter-wave Radio Signals Utilizing Measured Radio Channel Parameters

Sigurd S. Petersen, Oskar K. Feldstedt, Khadar Guled
Aalborg University
Department of Electronic Systems
Denmark
{sp19, ofelds19, kabdig19}@student.aau.dk

Wei Fan
Aalborg University
Department of Electronic Systems
Denmark
wfa@es.aau.dk

***Abstract*—Radio waves are invisible to humans, yet visualization of radio waves is important for many purposes. In this work, two wideband channel sounding systems, i.e. one mechanical steering horn antenna based on turntable, and the other electronic steering phased-array antennas, are developed to record radio channel parameters at millimeter-wave (mmWave) bands 28-30 GHz. The measured radio channel parameters are then used to reconstruct the mmWave radio signal trajectories. Dedicated measurements are then designed, e.g. path blocking with humans and path generation with metallic reflector, to validate the reconstructed mmWave signal trajectories. Our validation measurements demonstrate that visualization of millimeter-wave radio signal paths is feasible based on a few key channel parameters, i.e. power, delay and angle per path, which are collected by the measurement systems. This work is based on an undergraduate student project carried out in Aalborg University, Denmark.**

***Index Terms*—Antenna in Package (AiP) phased array, beam-steering, channel measurement, mmWave propagation**

I. Introduction

Understanding of radio waves and their trajectories is important for system development and optimization. Moreover, it is also of educational importance since better knowledge of radio waves and their trajectories can help mitigate public fear of radio technology. One example of public fear of radio technology and conspiracy theories of 5G was during the COVID-19 pandemic when these believers were lack of education correlates with this conspiracy [1]- [3]. This misinformation could be mitigated with the knowledge of visualizing radio waves since it helps people to know the physics of invisible matter.

As explained, it is not possible to see radio signal with human eyes because it operates on the invisible wavelength. However, several efforts have been taken to make it possible to visualize the trajectories of radio communication [4]- [8].

In [4] the effects of placing a human between a mmWave link were seen. It shows that a human can have significant effects on a mmWave 5G signal strength. The study focused on short indoor 5G links. In [5], [15]–[17] a experimental approach to characterize the radiochannel in multiple indoor scenarios was reported. It shows that the parameters are closely related to the size of the room, where the experiment is conducted. In [6] an effort to investigate the parameters of the multipath channel was made, using a high resolution propagation estimation (HRPE) algorithm to investigate composite channel characteristics, cluster-level characteristics and dynamic behaviors in an indoor scenario at 28-30 GHz. Efforts towards visualization have also been made. In [7] and [8] efforts to visualize the coverage of 5G signals have been made. [7] has focused on 3D heat mapping and [8] has focused on real time heat mapping in an outdoor scenario.

In radio communication, multipath is the effect which leads to radio signal reaching the receiver by more than one path [10]. In principle, with knowledge of the multipath parameters, i.e. direction of departure, direction of arrival, power and delay, and propagation environment database, one can reconstruct the path trajectory. For mmWave communications, only dominant propagation paths, e.g. line-of-sight paths, reflection or diffraction path of first orders are of main interest. Therefore, in principle it is possible to reconstruct the dominant mmWave signal paths once the knowledge of the channel parameters of the few dominant paths are obtained.

The rest of this paper is organized as follows. Section II measurement setup and campaign. Section III presents the measurement results with subsection A that contains comparison of two scenarios and section B the conclusion of these measurements. In this work, two experimental setups were developed for path trajectory reconstruction: the first one is a mechanical beam-steering which uses a turntable to rotate a horn antenna, and the second is an electronic beam-steering antenna that uses a 4 x 4 phased array antenna [11]. A vector network analyzer (VNA) is used to record the channel parameters, and then the data is processed in Matlab. The channel impulse response (CIR), power angle profile (PAP), and power angle delay profile (PADP) are obtained from the measured data [9].

Both experiment setups consist of two antennas, an omnidirectional transmitter antenna and a directional receiver antenna (either mechanic-steering or electronic steering), with the main path being the line of sight (LOS) path between the two antennas. LOS path should have the strongest signal power and the shortest time in the time domain. The LOS path is verified by blocking the anticipated LOS signal and then looking at the power change on channel impulse response. Furthermore, by introducing the metal plate, the transmitted signal is reflected upon the metal plate and to the receiver.

The reflecting path will lose some of its initial power when the signal is reflected and bent to the receiver, and therefore the distance and time delay compared to the LOS path will be longer. The verification process is also done by blocking the detected reflecting path in the measurements.

II. Measurement setup and campaign

For this work, we concentrate on the dominant propagation paths at mmWave bands. Therefore, our objective is to obtain the channel parameters, power, angle, delay for each path at one side of the communication link for the dominant paths. With a wider channel sounding frequency band, we have higher delay resolution, which means we are more capable of separating multipaths in the delay domain. Similarly, with a larger antenna aperture, we can achieve higher spatial resolution, meaning that we are more capable of separating multipaths in the spatial domain.

A. Measurement setup

The measurement system consists of a Tx antenna, an Rx antenna, and a vector network analyzer (VNA).

An omnidirectional bi-conical antenna is used as the transmitter (Tx) antenna as shown in Fig. 1. The operating frequency range is 2-30 GHz. The bi-conical antenna has an omni-directional antenna in the H-plane, and the half-power beamwidth (HPBW) in the E-plane is around 14 degrees at 28 GHz [12].

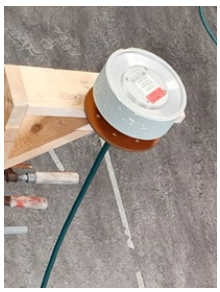

Fig. 1. Omnidirectional antenna as the transmitter antenna in both experiments.

The receiver antenna for mechanical beam-steering is a standard gain horn (SGH) of model 22240-20, with a wide frequency band ranging from 26.4 to 40.1 GHz, as shown in Fig. 2. The HPBW is around 15 degrees at 28 GHz for the H-plane and E-plane, respectively [13] [14]. The horn antenna is mounted on a turntable which can rotate 360° with adjustable steps, and this experiment setup will only scan the azimuth angle.

The last receiver antenna is a phased array antenna, where the elements can be controlled to form a beam of radio waves that can steer the beam, without physically moving the antenna. In this experiment, the antenna used is a 4 x 4 phased array antenna, as seen in Fig. 3 [11]. The phased array can steer its beam both in the azimuth and elevation domain. It can steer its beam from 0° to 180°, with a step of 5.625°. Taking into account that it has 33 beams in each direction, the whole AiP has 132 beams. The electronic beam-steering has been implemented in order to compare the results obtained with the mechanical beam-steering, therefore the AiP measurements only include beam-steering in the azimuth plane. The frequency is swept from 28 - 30 GHz with 3001 frequency points in the VNA.

Fig. 2. Horn antenna as the receiver antenna in mechanical beam-steering experiment.

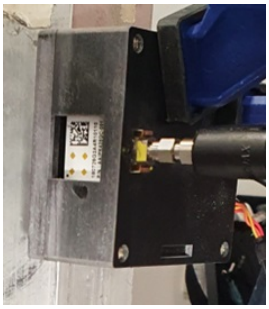

Fig. 3. 4 x 4 phased array antenna as the receiver antenna in electronic beam-steering experiment.

B. Software control

The measurement system is fully automated. For the mechanical steering system, the developed automatic software allows us to specify the step and range of rotation and it is possible to automate the process of recording and measuring data for each given step. We can also customize the waiting time to stabilize the rotating turntable before measurement. The rotation step is set to 4 degrees and the range is set to 360 degrees, which results in a total of 91 measurements.

For the electronic beam-steering experiment, phased array software is utilized to control the AiP elements simultaneously. The phase shift is set to 5.625 degrees and the range is set to 180 degrees, which results in a total of 132 measurements [11].

C. Measurement environment

1) Measurement scenario: All the measurements were performed at the Aalborg University antenna laboratory. The setup of the mechanical beam-steering experiment and its environment can be seen in Fig. 4, where a transmitter (denoted as nr. 1) is the omnidirectional antenna, and the receiver antenna (denoted as nr. 2) is the horn antenna that

can be rotated by the mechanical turntable (denoted as nr. 3), which is controlled by a laptop. To create some reflected signals, a metal plate was intentionally placed as a reflector (denoted as nr. 4). For recording the measurements, a VNA (denoted as nr. 5) was used. The distance between the Tx and Rx antenna is measured to be 1.85 m. For the electronic

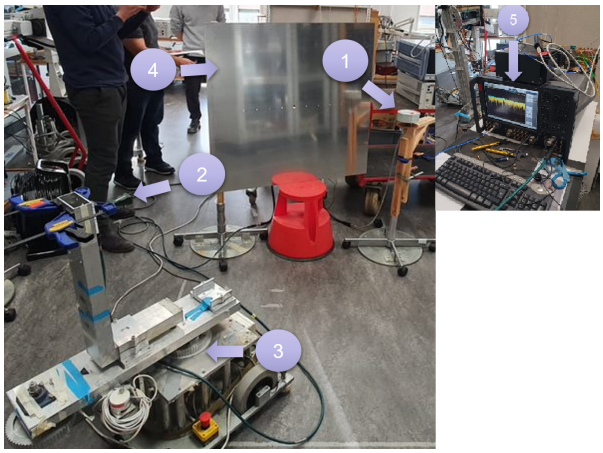

Fig. 4. Setup of mechanical beam-steering experiment.

beam-steering, the setup and its environment can be seen in Fig. 5, where nr. 1 is the same transmitter antenna as used in the mechanical beam-steering setup and in the same position. Then the receiver is changed to the phased array antenna as nr. 2, which is controlled with the laptop nr. 3 and lastly the reflector as nr. 4.

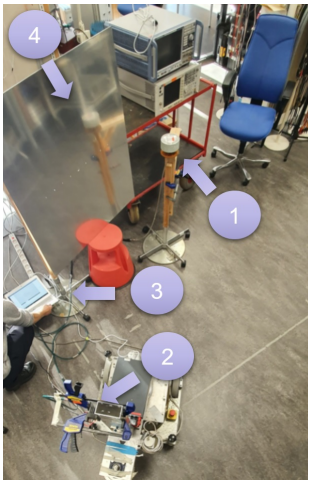

Fig. 5. Setup of electronic beam-steering experiment.

D. Measurement campaigns

1) Horn antenna as the Rx: An overview of all the measurements using the horn antenna as the receiver antenna is shown in Fig. 6. The first measurement is taken where the turntable is stationary at 0° and (a) without the reflector. This setup consists of two measurements, one without blocking the

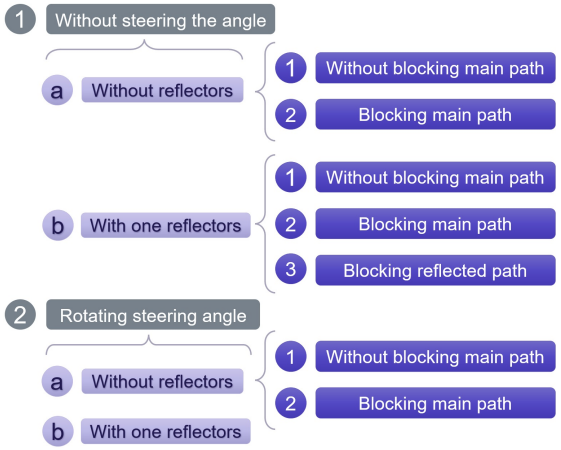

Fig. 6. Measurements overview of mechanical beam-steering experiment.

main path (LOS) and the other with the main path blocked. This simple measurement was designed to measure the LOS path and validate the estimated main path by blocking it with humans. Then the next one is with the reflector, where the reflected signal is introduced, and since the main path is presumed to be correct, then it is possible to find the angle of the reflected path by blocking the reflected path and confirming that the main path was indeed the correct one. Lastly, in part two, we aim to introduce spatial domain capability to detect the paths, where the turntable is rotating, (a) without a reflector and (b) with one reflector.

2) AiP antenna as the Rx antenna: Similarly, an overview of measurements performed with the AiP as the Rx antenna is shown in Fig. 7.

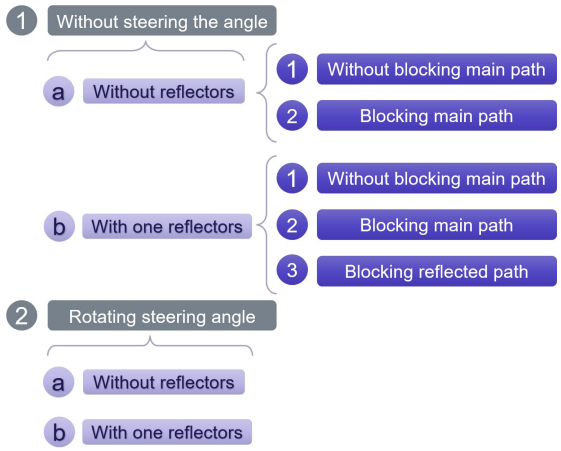

Fig. 7. Measurements overview of electronic beam-steering experiment.

3) Validation strategy of the paths: Validations of paths are done by blocking the main and reflecting signals using a human. As mentioned before the validation of each path is done by looking at the power in the time domain of each path. When the path has been blocked, the power of the signal should decrease and thereby confirming the trajectory of the path. By looking at the angle and the delay domain it is also

possible to distinguish between the LOS and reflected path since the LOS path has a shorter distance.

III. Measurement Results

1) Mechanical beam-steering measurements: As mentioned in Fig. 6, the first measurement is to find the LOS path and then confirm it by blocking the LOS path signal. The measured channel impulse response (CIR) can be seen in Fig. 8. The strongest path is -51.4 dB which is the anticipated LOS path when it is not blocked. When the anticipated LOS path is blocked the amplitude is reduced by 16.6 dB. Since the delay in x-axis is the same for the blocked one and unblocked one, it is confirmed to be the LOS path. Furthermore, the LOS path is 1.85 m, which corresponds well to the measurement distance between the Tx and Rx antenna, which was 1.89 m.

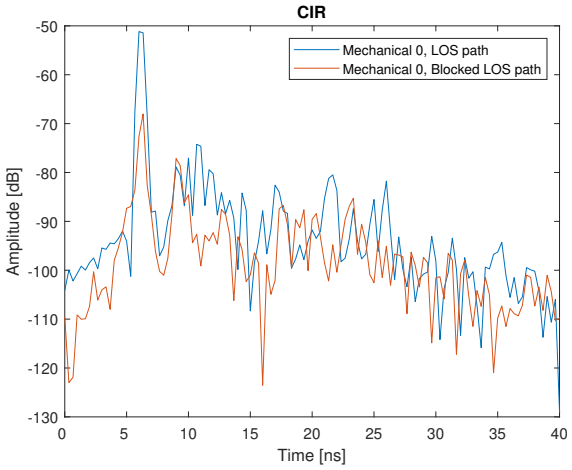

Fig. 8. Measured CIR for the LOS not blocked and blocked scenario without turntable rotation.

When the LOS path is found, the next step is to introduce a reflector to see if it is possible to identify and confirm the generated reflected signal. The metal plate is inserted to create the reflected signal as shown in Fig. 4 and the CIR is obtained as shown in Fig. 9.

Fig. 9 shows the LOS path is found at 6.3 ns. Then the reflecting path marked as the blue one has a power of -59.5 dB and when the reflecting path is blocked, the amplitude drops down to -76.9 dB. The mechanical beam-steering measurements for a fixed angle have then confirmed the LOS and reflecting path.

The next experiment is to rotate the horn antenna 360° by using the turntable and find which angle the LOS and the reflecting path has. Fig. 10 shows a power angle profile of both paths, where the LOS path is at 6.3 ns at 0° and a gain of -50.9 dB, and the reflected path is at 7.6 ns at -16° with a gain of -51.89 dB. Both paths were verified by blocking the signals.

In Fig. 10, both paths are close to each other in the angle domain, and it can be difficult to distinguish between the paths, so it can be necessary to improve the resolution of the separation/distinction of the two paths by improving the spatial

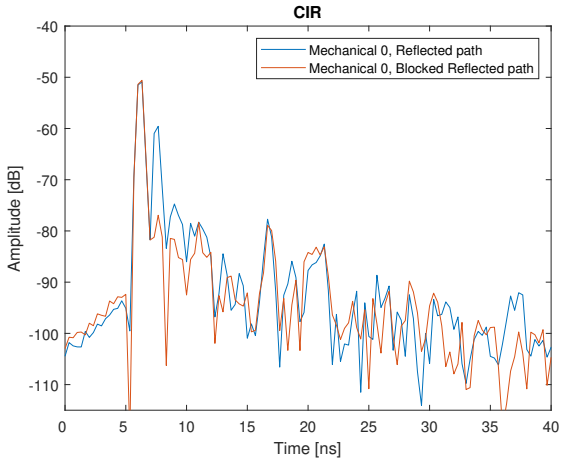

Fig. 9. Measured CIR for reflector scenario with not blocked and blocked paths without turntable rotation.

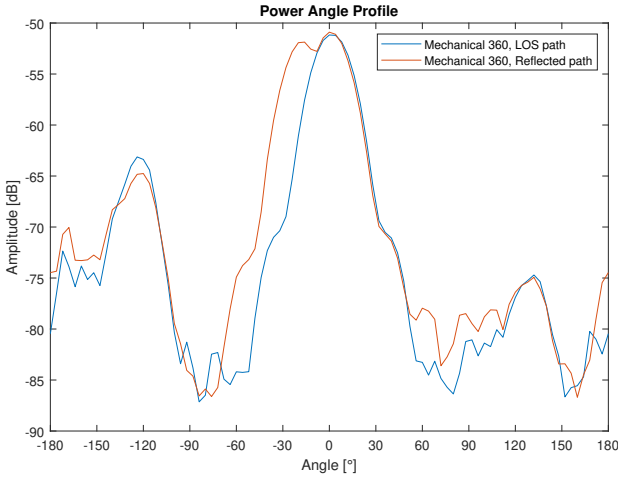

Fig. 10. Mechanical measurement where the turntable is rotating 360° and with LOS, reflected path.

resolution. There are two strategies, one way is to improve the current setup by using a narrower beam horn antenna or adding more array elements to the phased array to form a narrower beam. The second strategies to change into time domain, if the resolution in the spatial domain cannot be improved. Measured power angle delay profile (PADP) is shown in Fig. 11.

Fig. 11 shows two major signals, and before the experiments, the horn antenna was set to face the transmitter at 0°, and it is also the reason one of the signals is located at 0°. Looking at Fig. 8, it is also seen that the delay is consistent with the LOS path. A second distinguishing path was located at around -16°. This path has a time delay of 7.6 ns which matches with the path that was generated due to reflection, as seen in Fig. 9.

Since both paths were found with the knowledge of power, delay and angle for each path, it is possible to plot the trajectory for each path. These distances were also measured physically to cm accuracy, for instance the distance between the transmitter and receiver were 1.85 m and the measured

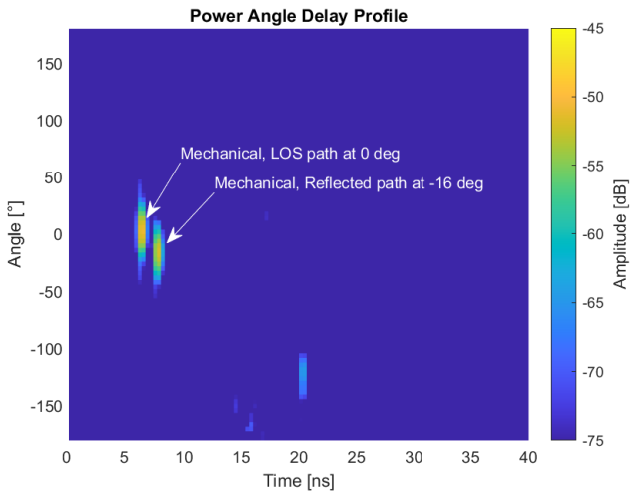

Fig. 11. PADP plot of the mechanical beam-steering.

one was 1.89 m.

2) Electronic beam-steering measurements: Using the method for the measurements summarized in Fig. 7, the first measurement with phased array is to find the LOS path, without a reflector and without steering the beam to verify the anticipated LOS path. The path is then blocked, just as before. Fig. 12 shows only one major peak in blue and when blocking the signal, the amplitude of the anticipated LOS path decreases, so it is the LOS path with time delay at about 6.6 ns.

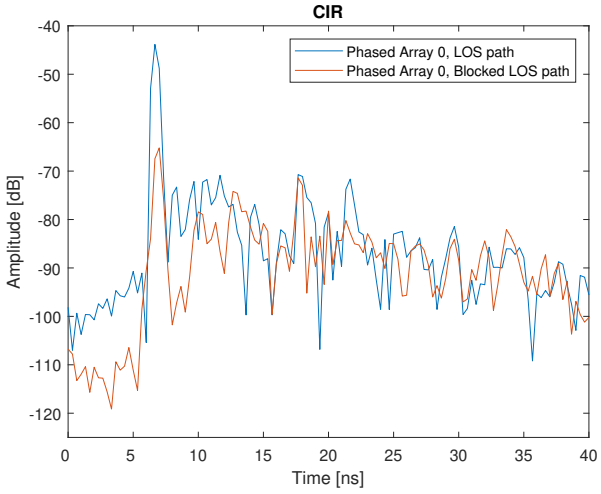

Fig. 12. Electronic beam-steering of LOS path with and without blocking the LOS path signal.

The next measurement is with a reflector and then finding the reflected signal and blocking the signal to see if the amplitude will decrease at the same time delay. The measurement can be seen in Fig. 13. Fig. 13 shows both the LOS path, and the reflected path at 8 ns and its amplitude at 48.8 dB. To verify it is the reflected path, it needs to be blocked and the measurements can be seen in Fig. 14. Fig. 14 shows the

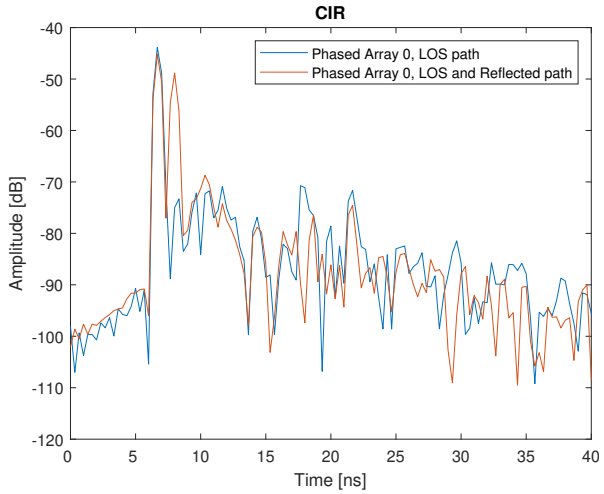

Fig. 13. Electronic beam-steering of LOS path and with/without the reflecting signal.

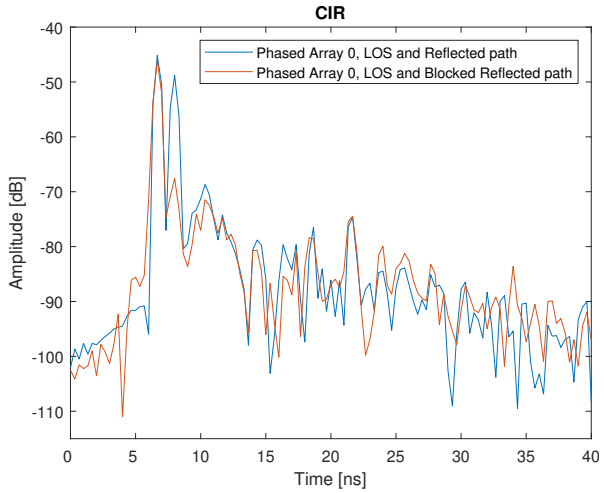

Fig. 14. Electronic beam-steering of LOS path and reflecting signal with and without blockage.

reflected path to be blocked and the amplitude is reduced with 18.3 dB, and the time delay is exactly the same, so it must be the reflected signal. As mentioned, both paths can also be seen by using the PADP as seen in Fig. 15. Fig. 15 shows two signals, and the turntable is at the same position, and the phased array antenna is sat about 4 cm to the left side from where the horn antenna was positioned, as shown in Fig. 5 as nr. 2. The beam-steering is facing the transmitter at 0º. Looking at the Fig. 15, the time delay is consistent with the LOS path with a time delay at 6.6 ns and is located at 0° and the second distinguished path is located at around -12°. This path has a time delay of 8 ns which matches with the path that was generated due to reflection as shown in Fig. 14.

Taking into consideration that the key parameters have been found through the measurements, it is then possible to plot the trajectory. These distances were also measured to cm accuracy. For instance the distance between the transmitter and receiver

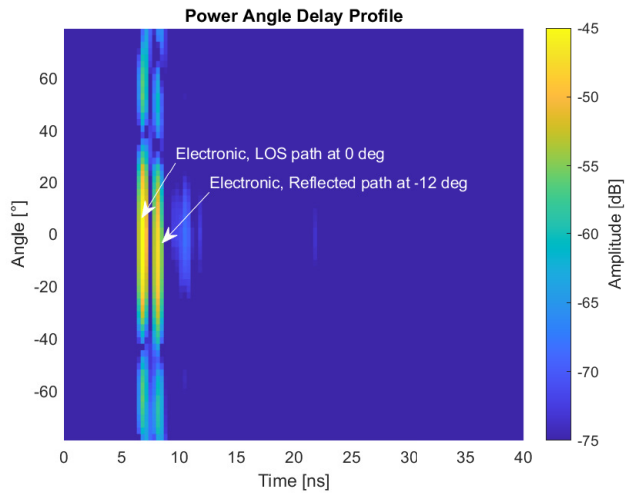

Fig. 15. PADP plot of the electronic beam-steering showing LOS path and reflecting signal.

were physically measured to 1.98 m and the calculation in reference to the measurements was 2.0 m. For the reflected path, the distance was measured physically to 2.4 m and the calculation in reference to the measurements was also 2.4 m.

IV. Conclusion

The objective of this work was to identify and verify the main path and the reflected path in both mechanical and electronic beam-steering scenarios, and then compare and validate the mechanical measurements against the electronic beam-steering. Furthermore, we aimed to compare the physical distance with the measured distance and plot the ray trajectories of the main path and the reflected path. In mechanical beam-steering as well as in electronic beam-steering, the main and reflected paths were identified and verified by blocking the signal path. The main path for the mechanical was 6.33 ns, whereas the electronic was 6.66 ns with a difference of 0.33 ns. The reflected signal for mechanical steering measurement is at 7.66 ns, whereas the electronic was 8 ns with a difference of 0.34 ns. These differences are very small as expected and correlate to the difference in placement of the phased arrayl.

The PAP in Fig. 10 shows the main path at 0 deg and the reflected path at -16 deg for the mechanical beam-steering. Comparing Fig. 10 against the PADP for the mechanical beam-steering, they are exactly the same when measuring in the center of each path at the PADP. Now looking at the differences between mechanical and electronic PADP plots, both main paths are the same at 0°, and the reflection path for mechanical is -16°, and electronic -12°, which is a -4° difference, which is expected since CIR showed about 10 cm in difference in distance and about 4 cm difference in placement of the phased array. Overall, through the measurements, it is confirmed that since the three key parameters are found, it is feasible to visualize the trajectory of mmWave radio signals.

References

[1] J. van Prooijen, “Why Education Predicts Decreased Belief in Conspiracy Theories”, November, 2016.

[2] Jolley ,Daniel and Paterson, Jenny L., Pylons ablaze: Examining the role of 5G COVID-19 conspiracy beliefs and support for violence, vol. 59. British Journal of Social Psychology, pp. 628-640, July, 2020.

[3] W. Ahmed et.al., ”COVID-19 and the 5G Conspiracy Theory: Social Network Analysis of Twitter Data”, Journal of Medical Internet Research, vol. 22, pp. 1201-1209, May, 2020.

[4] Dalveren, Y.; Karatas, G.; Derawi, M.; Kara, A. A Simple Propagation Model to Characterize the Effects of Multiple Human Bodies Blocking Indoor Short-Range Links at 28 GHz. Electronics 2021, 10, 305. https://doi.org/10.3390/electronics10030305

[5] Zhang, Guojin; Saito, Kentaro; Fan, Wei; Cai, Xuesong; Hanpinitsak, Panawit; Takada, Jun-Ichi and Pedersen, Gert Frølund, ”Experimental Characterization of Millimeter-Wave Indoor Propagation Channels at 28 GHz,” in IEEE Access, vol. 6, pp. 76516-76526, 2018, doi: 10.1109/ACCESS.2018.2882644.

[6] X. Cai, G. Zhang, C. Zhang, W. Fan, J. Li and G. F. Pedersen, ”Dynamic Channel Modeling for Indoor Millimeter-Wave Propagation Channels Based on Measurements,” in IEEE Transactions on Communications, vol. 68, no. 9, pp. 5878-5891, Sept. 2020, doi: 10.1109/TCOMM.2020.3001614.

[7] H.A. Sulaiman, M. A. Othman, M. M. Ismail and M. H. Misran, ”Wireless network visualization in 3D virtual environment framework,” 2012 21st Annual Wireless and Optical Communications Conference (WOCC), 2012, pp. 170-174, doi:10.1109/WOCC.2012.6198177.

[8] M. Inomata, T. Imai, K. Kitao and T. Asai, ”Radio Wave Visualizer for 5G New Radio Signal,” 2019 International Symposium on Antennas and Propagation (ISAP), 2019, pp. 1-3.

[9] Hejselbæk, J., Ji, Y., Fan, W., & Pedersen, G. F. (2017). Channel Sounding System for MM-Wave Bands and Characterization of Indoor Propagation at 28 GHz. International Journal of Wireless Information Networks, 24(3), 204-216.

[10] National Communications System Technology and Standards Division, ”Federal Standard 1037C - Telecommunications: Glossary of Telecommunication terms”, pp. 262-264, August, 1996.

[11] Gao, H., Wang, W., Fan, W., Zhang, F., Wang, Z., Wu, Y., Liu, Y., & Pedersen, G. F. (2020). Design and Experimental Validation of Automated Millimeter-Wave Phased Array Antenna-in-Package (AiP) Experimental Platform. IEEE Transactions on Instrumentation and Measurement, 70, [9199297].

[12] A-INFO, ”SZ-2003000/P - 2.0-30.0 GHz Bi-Conical Antenna”, URL:https://www.ainfoinc.com/amfilerating/file/download/file_id/4508/?fbclid=IwAR2qMNgSdvN7E4rqR3THYMOS9F9Od3oqnlY5M8Jj7ivAhrT-yeQgUtL3DIM (Accessed 15/06/22).

[13] Over-the-air characterization of millimeter-wave integrated antenna systems,”A. J. van den Biggelaar”,pp. 77, ISBN: 978-90-386-5125-5, URL: https://pure.tue.nl/ws/portalfiles/portal/163703182/20201111_Biggelaar.pdf?fbclid=IwAR3vQjlLXG1iKktO0FMA9Z3XA0DQQ7JT0oUPy-xzxDDudQGBdkl g70V1Ok (Accessed 15/06/22)

[14] FLANN Microwave, ”STANDARD GAIN HORNS SERIES 240”, pp. 1-2 URL: https://flann.com/products/antennas/standard-gain-horns-series-240/ (Accessed 15/06/22)

[15] J. Hejselbæk, J. Ø. Nielsen, W. Fan and G. F. Pedersen, ”Measured 21.5 GHz Indoor Channels With User-Held Handset Antenna Array,” in IEEE Transactions on Antennas and Propagation, vol. 65, no. 12, pp. 6574-6583, Dec. 2017, doi: 10.1109/TAP.2017.2742556.

[16] F. Zhang, W. Fan and G. F. Pedersen, ”Frequency-Invariant Uniform Circular Array for Wideband mm-Wave Channel Characterization,” in IEEE Antennas and Wireless Propagation Letters, vol. 16, pp. 641-644, 2017, doi: 10.1109/LAWP.2016.2594488.

[17] Y. Ji, W. Fan and G. F. Pedersen, ”Channel Characterization for Wideband Large-Scale Antenna Systems Based on a Low-Complexity Maximum Likelihood Estimator,” in IEEE Transactions on Wireless Communications, vol. 17, no. 9, pp. 6018-6028, Sept. 2018, doi: 10.1109/TWC.2018.2854553.